



UKAEA-CCFE-PR(25)344

E. Parr, K. G. McClements, C. A. Michael, S. Y. Allan, M. Cecconello, A. R. Jackson, C. Vincent, T. Wilson, R. Worrall

Studying spacial distributions of fusion within MAST-U using Fission-Chamber Array measurements

Enquiries about copyright and reproduction should in the first instance be addressed to the UKAEA Publications Officer, Culham Science Centre, Building K1/0/83 Abingdon, Oxfordshire, OX14 3DB, UK. The United Kingdom Atomic Energy Authority is the copyright holder.
The contents of this document and all other UKAEA Preprints, Reports and Conference Papers are available to view online free at scientific-publications.ukaea.uk/

Studying spacial distributions of fusion within MAST-U using Fission-Chamber Array measurements

E. Parr, K. G. McClements, C. A. Michael, S. Y. Allan, M. Cecconello, A. R. Jackson, C. Vincent, T. Wilson, R. Worrall



PAPER • OPEN ACCESS

Studying spatial distributions of fusion reaction rates within MAST-U using fission-chamber array measurements

To cite this article: E Parr et al 2025 Plasma Phys. Control. Fusion 67 075035

View the article online for updates and enhancements.

You may also like

- <u>Multiphysics approach to plasma neutron</u> <u>source modelling at the JET tokamak</u>
 Žiga Štancar, Marina Gorelenkova, Sean Conroy et al.
- Statistical validation of predictive TRANSP simulations of baseline discharges in preparation for extrapolation to JET D—T Hyun-Tae Kim, M. Romanelli, X. Yuan et al
- 1997 JET DT experiments revisited—comparative analysis of DD and DT stationary baseline discharges Hyun-Tae Kim, A.C.C. Sips, C.D. Challis et al.

Plasma Phys. Control. Fusion 67 (2025) 075035 (8pp)

Studying spatial distributions of fusion reaction rates within MAST-U using fission-chamber array measurements

E Parr^{1,*}, K G McClements¹, C A Michael², S Y Allan¹, M Cecconello^{3,4}, A R Jackson⁵, C Vincent¹, T Wilson¹ and R Worrall¹

- ¹ UKAEA (United Kingdom Atomic Energy Authority), Culham Campus, Abingdon, Oxfordshire OX14 3DB, United Kingdom
- ² University of California Los Angeles, Los Angeles, CA 90095-7099, United States of America
- ³ Department of Physics, Durham University, Durham DH1 3LE, United Kingdom
- ⁴ Department of Physics and Astronomy, Uppsala University, Uppsala SE-75105, Sweden

E-mail: Edward.Parr@ukaea.uk

Received 17 February 2025, revised 25 April 2025 Accepted for publication 3 July 2025 Published 23 July 2025



Abstract

By analysing the neutron rates measured using multiple fission-chamber (FC) diagnostics—constituting a FC array (FCA)—the spatial distribution of fusion reaction rates within a tokamak may be studied. Using the two-FC set-up at Mega-Ampere Spherical Tokamak Upgrade, analysis methods are presented for both the study of poloidal neutron emissivity distributions and neutral-beam injection shine-through measurements. Different FCA configurations are also proposed, with the possible future uses for these diagnostics discussed.

Keywords: neutrons, fast-ions, fission chamber, neutron emissivity distribution, NBI

1. Introduction

Fission-Chamber (FC) diagnostics produce signals proportional to the incoming neutron flux, which may be scaled to give total neutron rates produced from fusion reactions in a tokamak. To account for changes in FC detection efficiency which may arise from variations in the plasma position and shape, multiple FCs have previously been employed to measure total neutron rates [1–3]. Presently, however, it is conversely proposed that by analysing data from multiple FCs simultaneously—in a FC Array (FCA)—information

Original Content from this work may be used under the terms of the Creative Commons Attribution 4.0 licence. Any further distribution of this work must maintain attribution to the author(s) and the title of the work, journal citation and DOI.

about the spatial distribution of fusion reactions may be inferred, allowing for a variety of features and phenomena of magnetically-confined plasmas to be studied.

The Mega-Ampere Spherical Tokamak Upgrade (MAST-U) [4] has an array of two toroidally-displaced FCs operated in current mode [5], the positions of which are given on the toroidal cross-section shown in figure 1. Figure 2 shows time traces from a MAST-U discharge (shot 46943), with on- and off-axis neutral-beam injection (NBI) power (a) and total neutron rates, I (s⁻¹), measured by the two FCs (b). The raw current signal from the FCs is produced by high-energy fission fragments from the decaying ^{236m}U—produced following neutron capture of ²³⁵U—impinging on the ionising gas. The I rates are then obtained by applying a low-pass filter for noise reduction and a background subtraction to the raw signal, before the application of three constant scaling coefficients [6]. Firstly, the current signal is converted to a neutron flux incident on the FC using a coefficient provided by the manufacturer. Secondly, the flux is converted to a total neutron

⁵ Department of Physics, Florida International University, Miami, FL 33199, United States of America

^{*} Author to whom any correspondence should be addressed.

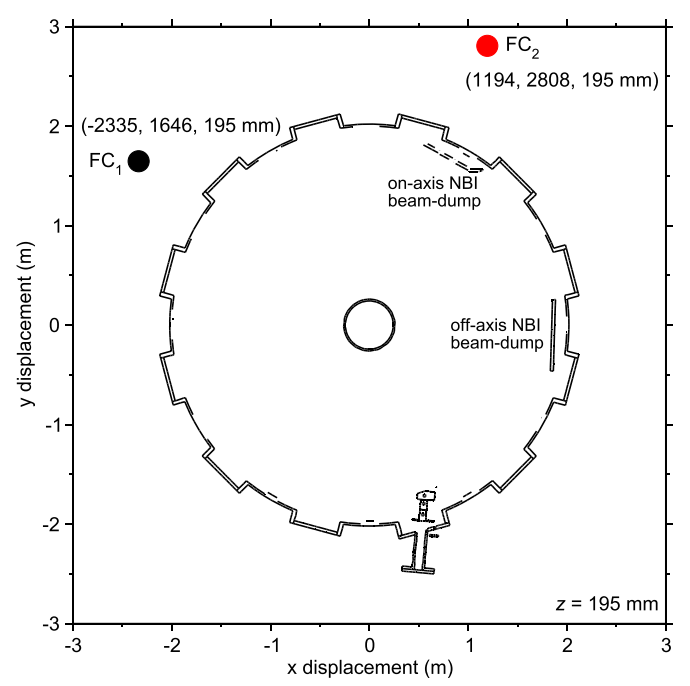


Figure 1. Toroidal cross section of the Mega-Ampere Spherical Tokamak Upgrade (MAST-U) at a vertical displacement of z = 195 mm. The positions of the two fission chambers, FC₁ and FC₂ (black and red filled circles, respectively), and the on- and off-axis NBI beam-dumps are highlighted.

emission rate in the plasma by considering the geometry and neutron transmission efficiencies of the MAST-U and FC setups. These coefficients, different for the two FCs, were found using Monte-Carlo Neutron-Particle (MCNP) simulations of 2.45 MeV neutrons (produced in D-D fusion reactions) emitted from a typical on-axis spatial distribution. Finally, the third scaling coefficient calibrates the measurement by correcting for discrepancies found between neutron rates measured using activation foils and those calculated from MCNP simulations. These final simulations used total emission rates found by applying the first two correction coefficients to the FC data. Although the second coefficient assumes a spatial distribution of neutron emissivity unchanging with time (referred to as static), in reality shifts in this distribution can occur, producing differences in the relative detection efficiencies of the two FCs. A measure sensitive to changes in the distribution may therefore be obtained by taking the ratio of the neutron rates measured using the two fission chambers,

$$r = \frac{I_2}{I_1}. (1)$$

Shifts in r are then indicative of a change to the distribution of fusion reaction rates, whereas varying neutron rates of a static distribution will result in a constant r. For convenience, and to measure deviations in the neutron emissivity distribution relative to that of a given discharge, r is normalised to a constant value, r_0 : giving $r' = r/r_0$. The value for r_0 presently used is from an NBI-heated discharge using both on- and off-axis beams, and is the mean r value between 0.4 and 0.8 s for shot 46 943. The time evolution of r' for plasma discharge 46 943

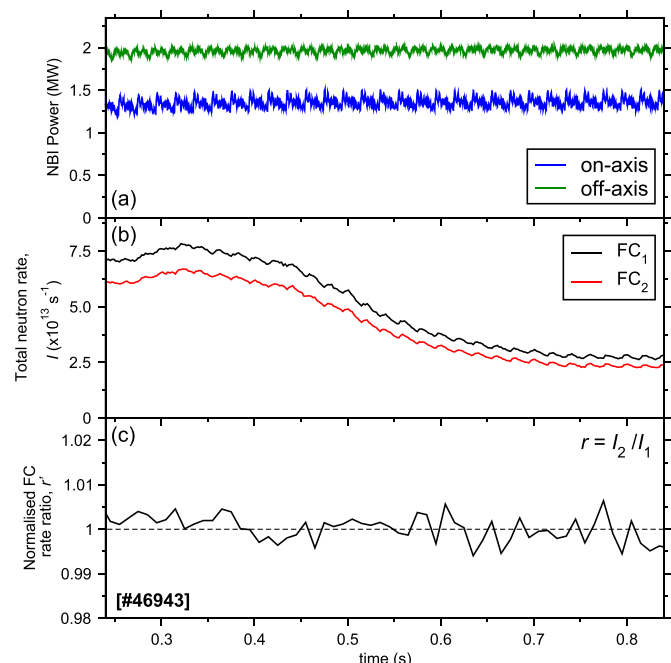


Figure 2. FCA time traces from an NBI-heated discharge (shot 46943). Panel (a) shows NBI heating power from on- and off-axis beams, Panel (b) the total neutron rates, I, measured in FCs 1 and 2, and Panel (c) the ratio between these rates, $r = I_2/I_1$, normalised to a constant value to give r'.

is shown in Panel (c) of figure 2 for the I rates from Panel (b). The binning time scale has been increased in Panel (c) compared with (b) to remove statistical variations in the r' values deriving from the FC signals. Here, a constant r' is consistent with a static distribution, even as the total neutron rate varies.

Two applications for the FCA are presented in the following sections: studying poloidal neutron emissivity profiles, and measuring NBI shine-through. In a final section possible configurations of, and improvements to, future FCA set-ups are proposed, with reference to the diagnostic and experimental possibilities these would provide.

2. Poloidal neutron emissivity profiles

Changes to the poloidal neutron emissivity profile may be studied by measuring shifts in the FCA neutron-rate ratio, r', and comparing these to forward-modelled predictions obtained using MCNP simulations.

Simulations were performed using Version 6.2 of the MCNP code [7], with neutron cross-sections taken from the Fusion Evaluated Nuclear Data Library (FENDL-3.2 [8]). The model included the MAST-U vacuum vessel, along with its internal and support structures, the surrounding walls and platforms, as well as other permanent equipment such as the NBIs and FCs. Fluxes of neutrons reaching the two FCs were simulated using, as a source, a filamentary, toroidally-symmetric ring of 2.45 MeV neutrons set at varying (*R*,*z*) values. Figure 3 shows a poloidal cross-section of MAST-U with the locations of the neutron-source rings used in the MCNP simulations indicated. These neutron-source locations were chosen

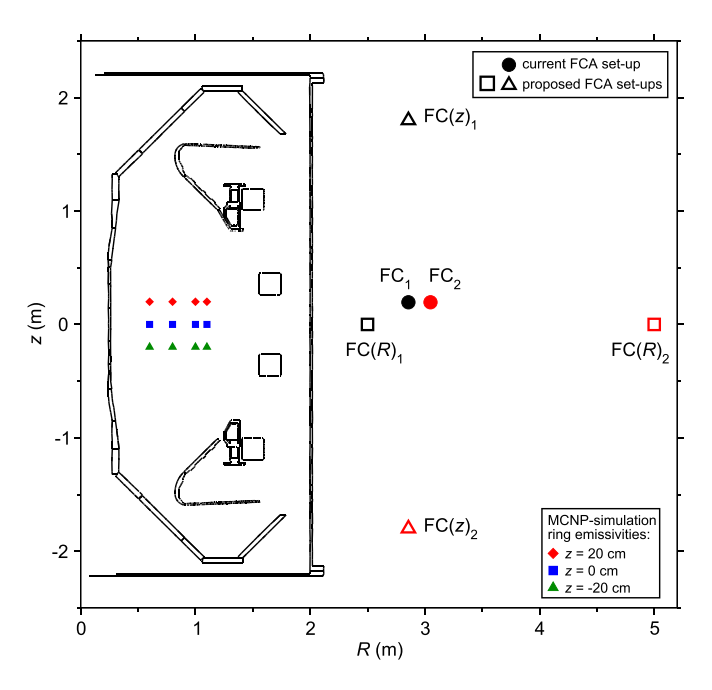


Figure 3. Poloidal cross-section of MAST-U with the R-z locations of the ring neutron emissivities used in MCNP simulations indicated: R = 60, 80, 100, 110 cm for z = 20 (filled red diamonds), 0 (filled blue squares), -20 cm (filled green triangles). The current positions on the R-z plane of the two fission chambers, FC₁ and FC₂ (black and red filled circles, respectively), are indicated. Also shown are two proposed pairs of FCs positioned to optimise their sensitivity to shifts in the R, FC(R)_{1,2} (black and red unfilled squares, respectively), and R, FC(R)_{1,2} (black and red unfilled triangles, respectively) of the emissivity distribution.

to cover typical regions of poloidal emissivity: allowing for measured r' values to be broadly correlated with profile positions. The simulated neutron-flux energy distributions incident at the FCs were integrated with the cross-sections for neutroncapture followed by fission of ²³⁵U to give values proportional to the expected signals in the two FCs. Figure 4 shows ratios of these predicted values, ρ' , as a function of the R of the emissivity ring for z = -20, 0, 20 cm. Here ρ' is the simulated equivalent of r', and has been normalised with respect to a value found using a realistic on-axis emissivity profile [centred at (R,z) = 92, 0 cm] typical of a two-beam heated plasma. The relative positions of the two FCs in the (R,z) plane are shown in figure 3, indicating a small R offset between the two diagnostics. A decreasing rate ratio would therefore be expected for increasing R of the neutron emissivity, due to the closer proximity of FC1 to the plasma. This trend, expected from purely geometric considerations, is observed in the simulated results of figure 4. However, the distribution of vessel components is also seen to have a significant effect on the relation between ρ' and (R,z).

Experimentally, the effects of changing poloidal neutron emissivity profiles on r' may be demonstrated by comparing plasmas produced using different heating regimes. The different neutron emissivity profiles produced by on- and off-axis NBI-heated plasmas on MAST-U have previously been studied in [9, 10] using TRANSP/NUBEAM

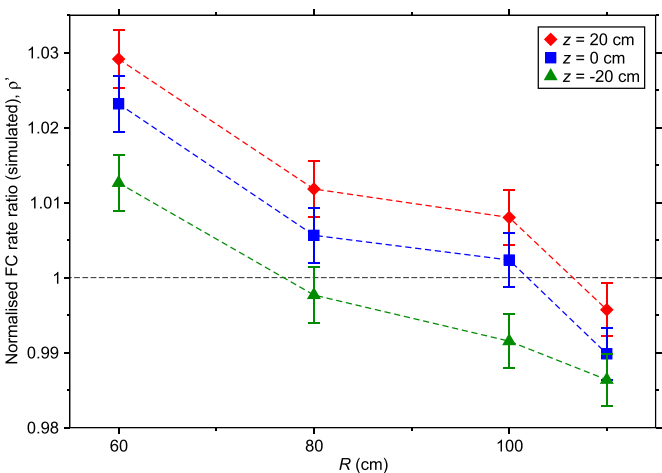


Figure 4. Predicted normalised FC rate ratios, ρ' , found using MCNP simulations using toroidally-symmetric, filamentary ring-emissivity distributions set at different plasma radii, R, and vertical displacements, z. Results have been normalised to a value found using a realistic on-axis [(R,z) = 92, 0 cm] emissivity distribution produced by a two-beam heated plasma.

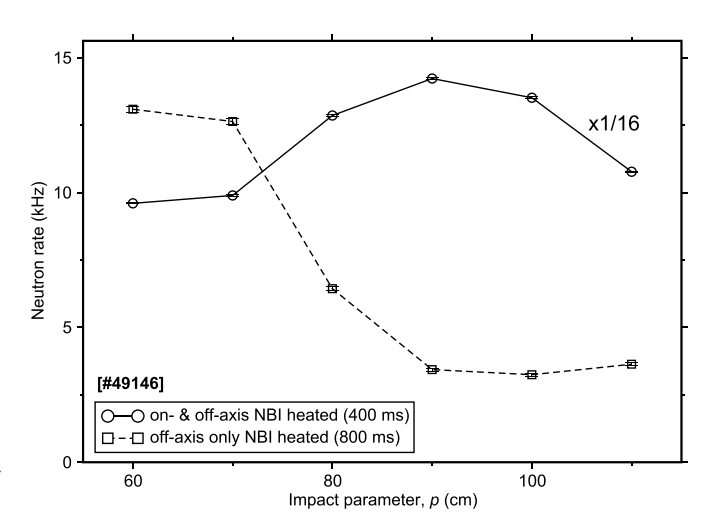


Figure 5. Neutron rates (with statistical errors) shown as a function of plasma impact parameter, *p*, measured in the NCU for on- and off-axis (400 ms) and off-axis only (800 ms) NBI-heated plasmas (shot 49146).

simulations [11, 12] and compared with experimental observations using the neutron-camera upgrade (NCU) [13]. These studies found emissivity profiles peaked around the core when on-axis heating was applied. For off-axis heated plasmas, hollow distributions with pronounced peaking on the inboard side were found. This peaking is due to the longer time spend by the fast ions on the high-field-side sections of their orbits. This is a result of magnetic-moment conservation, whereby velocity transfers from the parallel to the perpendicular components, with respect to the toroidal magnetic field, when moving to the higher-field side. Data from a typical discharge consisting of on- and off-axis, followed by off-axis only, NBI heating (shot 49146) are shown in figures 5 and 6 from the NCU and

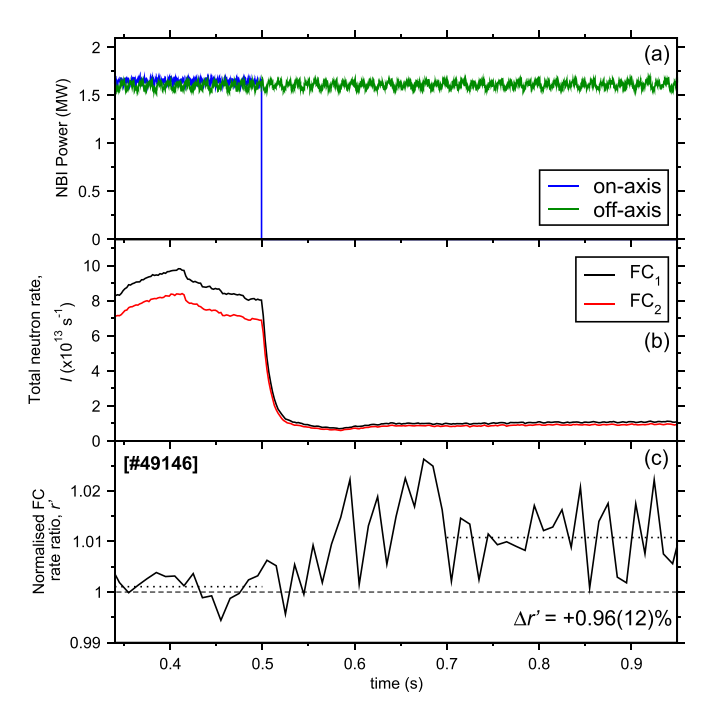


Figure 6. FCA time traces from an on- and off-axis (up to $500 \, \mathrm{ms}$) and off-axis only (from $500 \, \mathrm{ms}$) NBI heated plasma discharge (shot 49146). Traces shown same as figure 2. The averaged r' values are shown as dotted lines for time periods within the two different heating regimes (0.35–0.5 s and 0.7–0.95 s); with the change in ratio, $\Delta r'$, given.

FCA, respectively. It should be noted that due to the much larger fusion rate produced by on-axis heating (\sim x10 that of offaxis), the emissivity profile is largely determined by on-axis heating in two-beam plasmas. The NCU results, giving line-integrated neutron rates measured as a function of impact parameter, p, indicate a shift in the centre of the neutron emissivity profile from $R \sim 90$ to 60 cm between the two heating regimes (although changes in z of emissivity cannot be determined). A shift in r' of +0.96(12)% is observed between the two heating regimes (between 0.34-0.5 s and 0.7-0.95 s). Considering the trends of the forward-modelled ρ' values this shift is consistent with the observed change in R of emissivity from the NCU data, as well as the emissivity profiles predicted using TRANSP/NUBEAM for on- and off-axis heated plasmas in [9, 10].

3. NBI shine-through measurements

As well as changes to the poloidal emissivity profile, shifts in the spatial distribution of emitted neutrons may also arise from the introduction of additional sources of fusion reactions. One example of this, which will be discussed, are the neutron sources produced by NBI shine-through fusion at the beamdumps. These neutron sources may be observed, and the shine-through producing them quantified, using the FCA.

NBI shine-through is constituted of NBI neutrals that do not undergo charge-exchange or ionisation, and therefore reach the opposite plasma-facing components. Beam-dumps are positioned at the end of the beam-lines and are designed to absorb this shine-through. On MAST-U the beam-dumps consist of both inner and outer tiles made from carbon-fibre composite and graphite, respectively. Background deuterium absorbed in these tiles may therefore undergo fusion reactions directly with the high-energy shine-through particles incident upon them. The different FCA r' values resulting from neutrons produced via fusion in the NBI beam-dump compared to those from fusion reactions in the plasma (where $r' \simeq 1$) may then be used to measure the proportion of shine-through. In this study only shine-through from the fullenergy beam fraction (E_{full}) will be considered. This is due to the much lower relative rates of beam-dump fusion reactions that are estimated to be produced by the half- (E_{half}) and third-energy (E_{third}) beam fractions using ion energyloss [14] with fusion cross-section [15] calculations: e.g. 97.9:1.8:0.3% (for E_{full} : E_{half} : E_{third}) of the total D+D \rightarrow ³He+n beam-dump fusion, for full shine-through of a 54.4 keV beam with 68:17:15% flux fractions (relative fractions of respective beam particles produced), assuming a uniform density of background deuterium within the beam-dumps.

FCA neutron rates deriving only from shine-through fusion may be studied and quantified using shots without plasma (i.e. beam-into-gas/vacuum) and where no toroidal magnetic field is applied ($B_t = 0$). For beam-into-gas shots, energy loss, scattering, and fusion of the NBI particles with the gas are neglected. Also, any NBI particles ionised in the gas will maintain their trajectories in the absence of a toroidal magnetic field. Beam-into-gas and into-vacuum shots will therefore be considered equivalent, with effectively all of the NBI deuterium reaching the beam-dumps (i.e. 100% shine-through). Figure 7 shows the FCA data from examples of such beam-into-gas (shot 47063) and beam-into-vacuum (shots 50138 and 50270) discharges. The FCA ratios measured for these shots for both on- and off-axis NBI beam-on periods are compared in table 1 with those from MCNP simulations using a point-source of 2.45 MeV neutrons located at the respective beam-dumps. As the observed and simulated values are consistent, it may be assumed that the total neutron rates and ratios measured are those deriving only from the fusion of 100% shine-through at the beam-dumps. The much larger r' value for on-axis compared with off-axis NBI results predominantly from the close proximity of FC2 to the on-axis beam-dump compared with FC₁, and the resulting inverse-squared intensity disparity produced in the detection efficiencies between the two FCs. As the contributions to total neutron rates from off-axis NBI shinethrough fusion are small compared with those from on-axis NBI, and r' is close to 1-resulting from neither FC having greatly enhanced sensitivity to off-axis beam-dump neutrons relative to the other-these contributions will be neglected and only on-axis shine-through will presently be discussed.

The proportion of full-energy NBI neutrals reaching the beam-dump in a plasma discharge is calculated using A.6 (the derivation of which is given in appendix). The quantities r' and I_2 are measured throughout the discharge, while constant values for the maximum total neutron rate in FC₂, $I_{0,b2}$, and rate ratio, r'_b , produced only by shine-through, at 100%, are determined from beam-into-gas/vacuum shots. The $I_{0,b2}$ value depends on both the characteristics of the NBI [beam energy

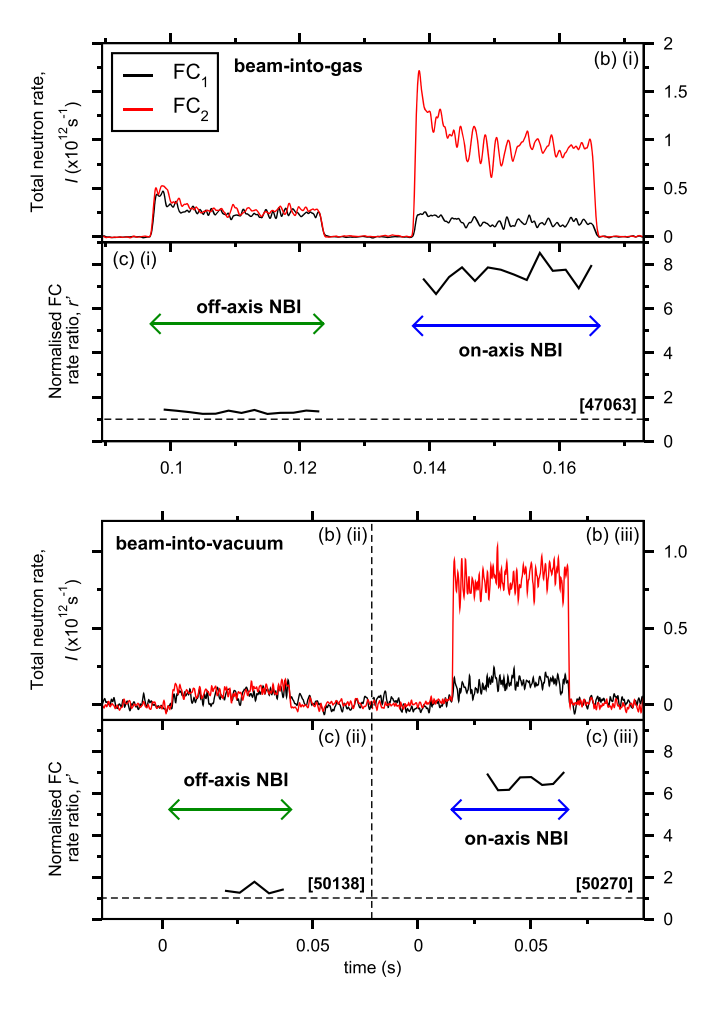


Figure 7. Time traces from beam-into-gas [shot 47063 (i)] and beam-into-vacuum [shots 50138 (ii) and 50270 (iii)] discharges with $B_t = 0$: giving 100% shine-through only. Traces shown are same as figure 2, excluding NBI power. The r' values are given only for times when NBI is applied (which are indicated), and when uncertainties from fluctuations close to the base-line are not too large.

Table 1. Comparison of measured r' and MCNP-simulated ρ' FCA ratio values deriving from beam-dump fusion. Measurements are taken from beam-into-gas (47063) and beam-into-vacuum [50270 (on-axis) and 50138 (off-axis)], $B_t = 0$, discharges (shown in figure 7) and simulations performed using a point-source of 2.45 MeV neutrons at respective beam-dumps.

	r' (gas)	(vacuum)	ho'
On-axis NBI	7.3 ± 0.5	6.7 ± 0.4	7.02 ± 0.03
Off-axis NBI	1.3 ± 0.1	1.4 ± 0.2	1.58 ± 0.01

 $(E_{\rm NBI})$, total flux, and flux fractions] and the concentration of D at the beam-dump. Figure 8 shows normalised FC₂ rates, I', measured for on-axis NBI beam-into-gas/vacuum shots taken during the MU02, MU03, and MU04 MAST-U experimental campaigns. These values have been normalised with respect to the NBI-dependent fusion rates. These were estimated from the $E_{\rm NBI}$ (using ion energy-loss [14] with fusion cross-section [15] calculations), along with the total flux and flux fractions. Despite this normalisation, a variation with

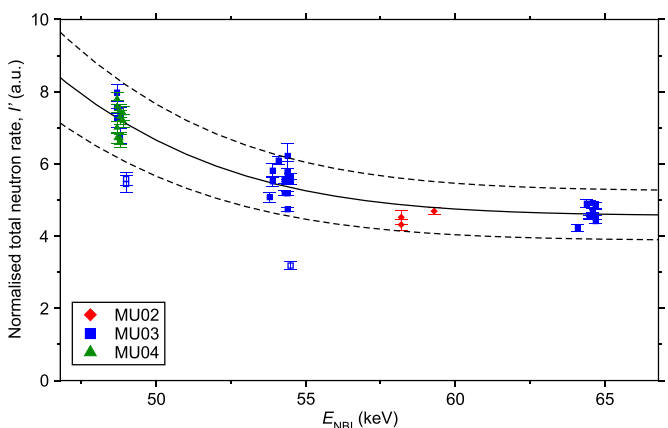


Figure 8. Total neutron rates measured in FC₂ normalised to beam-dump fusion rates estimated with respect to the NBI characteristics, I' (see text for details), shown as a function of on-axis NBI energy, $E_{\rm NBI}$. Data taken from on-axis NBI beam-into-gas/vacuum shots producing 100% shine-through. Discharges from across MAST-U campaigns MU02, MU03, and MU04, as indicated, have been used. The function used to determine $I_{0,b2}$ values from beam energies is given as a solid line, with uncertainties as dashed lines. The three outlying points, shown as open symbols, were not used in the fit.

respect to $E_{\rm NBI}$ is observed. An empirical fit has been taken (which is shown as a solid line with dashed uncertainty estimate) which can be used to determine an $I_{0,b2}$ value from the $E_{\rm NBI}$ used for the shot; this being renormalised back from the $I'(E_{\rm NBI})$ value from the fit. The three points anomalously separated from the others have not been included in the fit, and are shown as open symbols. The distribution of values about this fit are then assumed to derive from variations in the D concentrations at the beam-dump (as well as the uncertainties in the measurements). These variations introduce an estimated \sim 15% uncertainty in $I_{0,b2}$. However, more accurate determination of $I_{0,b2}$ may be achieved by considering beam-intogas/vacuum shots performed at similar times to the analysed shot. The same r'_{b} value is assumed for all shine-through fusion at a particular beam-dump, irrespective of shine-through fusion rate.

The estimates of shine-through measured by the FCA may be compared with results from two diagnostic systems currently at MAST-U which measure temperature increases at each beam-dump induced by shine-through. Each beam-dump has 32 embedded thermocouples, as well as two infra-red (IR) pyrometers positioned to measure the surface temperatures via the radiation emitted. Panels (a) of figures 9 and 10 show the line-integrated electron densities along the on-axis NBI beamline from Thomson-scattering (TS) measurements [16] during discharges where disruptions cause a dramatic drop in (shot 49147), and total loss of (shot 49257), plasma density, respectively. Data from the conventional monitoring systems are also shown (excluding thermocouple data for shot 49257), indicating the resulting shine-through, along with the on-axis NBI power. Results from the FCA are shown in Panels (b) and (c), with the shine-through induced fusion at the on-axis beamdump causing r' to increase [to between 1 and r'_b] following the drops in density. The shine-through, calculated from FCA

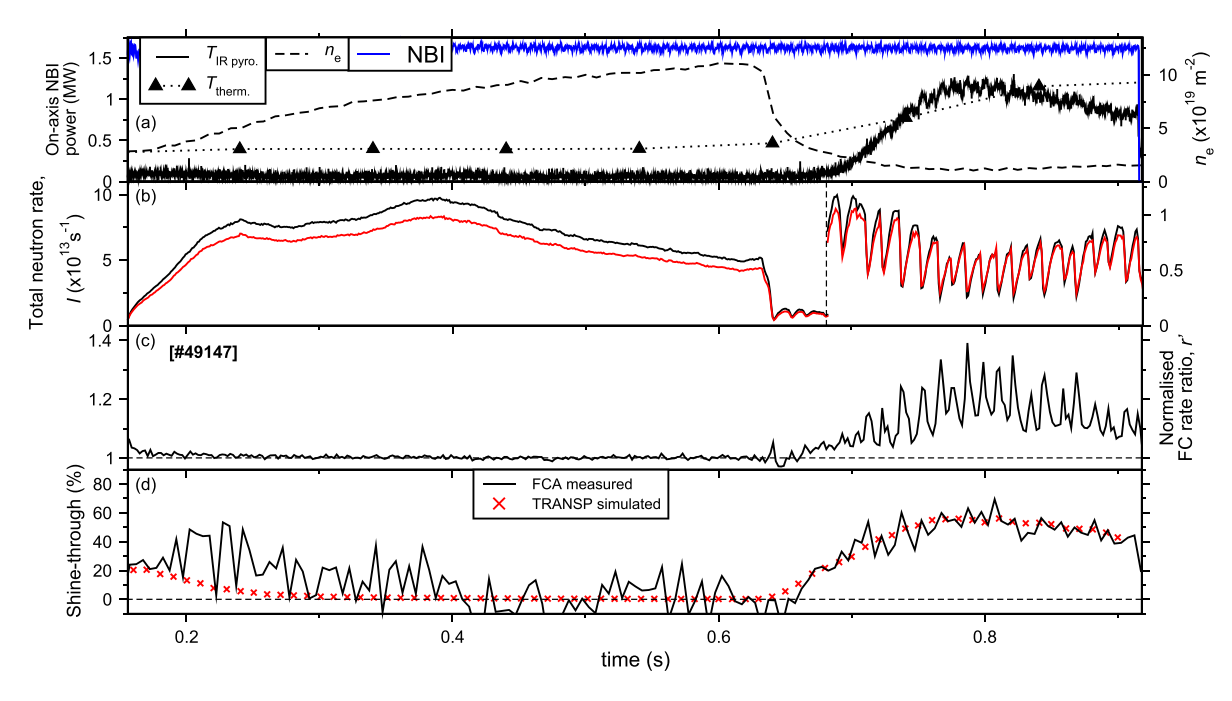


Figure 9. Time traces illustrating FCA measurements of on-axis NBI shine-through during a discharge with significant plasma density loss following a disruption (shot 49147). (a) Line-integrated electron density along on-axis NBI beam-line calculated using TS data, n_c ; measurements from the IR pyrometer ($T_{\rm IR \ pyro.}$) and embedded thermocouple ($T_{\rm therm.}$) of the on-axis beam-dump; and on-axis NBI power. (b) Total neutron rates measured in the FCs. (c) FCA ratios, r'. (d) Shine-through (%) of the on-axis NBI full-energy fraction measured using the FCA and predicted using TRANSP simulations.

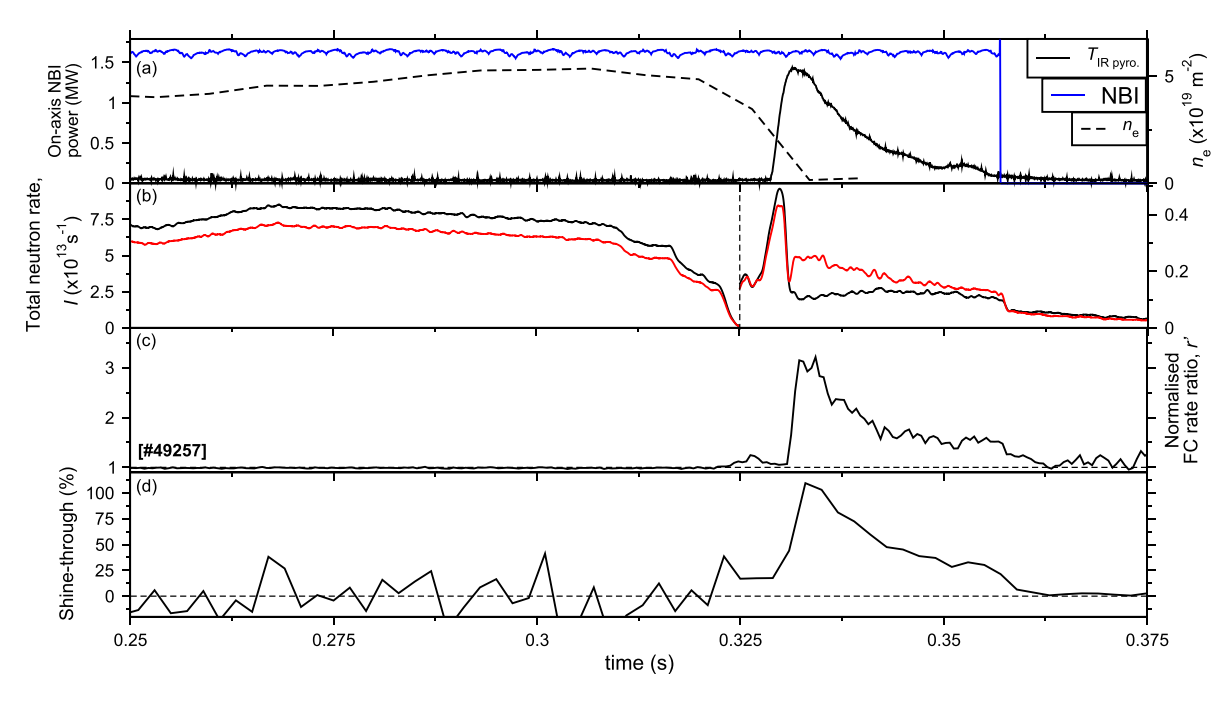


Figure 10. Time traces illustrating FCA measurements of on-axis NBI shine-through during a discharge with total plasma density loss following a disruption (shot 49257). Traces shown same as figure 9, excluding $T_{\text{therm.}}$ data and TRANSP-simulated shine-through.

data using A.6, is given in Panels (d). Qualitatively, there is excellent agreement between the data from the conventional diagnostic systems and the FCA measurements. It should be noted that during the periods of high neutron rate deriving from confined-plasma fusion during the flat-top phase it is observed that small uncertainties in the measured r' (statistical

and systematic) translate to large fluctuations, and deviations, in the shine-through measurements. These periods do, however, often coincide with negligible shine-through, as the high densities required to produce high confined-plasma fusion rates also act to deposit virtually the whole beam into the plasma.

The shine-through predicted using TRANSP simulations are compared with measured values for shot 49147 in figure 9(d). Excellent quantitative agreement is seen between the measured and predicted values, where a uniform $Z_{\rm eff}$ of 1.5 deriving from carbon impurities was assumed for the simulations. Changing $Z_{\rm eff}$ between 1 and \sim 2 was observed to have a negligible effect on the predicted shine-through. However, for higher values the associated reduction in shine-through may be matched with simulation to give a rough $Z_{\rm eff}$ measurement. Although large density drops such as this are not present in most discharges, comparisons with predicted shine-through may be made for each shot during the low-density start-up period (e.g. figure 9 time from 156 to 200 ms).

4. Future implementations and summary

For the study of poloidal neutron emissivity profiles the positions of the FCs may be optimised from those of the current set-up. Figure 3 indicates possible (R,z) locations of two pairs of FCs, FC(R) and FC(z), positioned to measure shifts in R and z of the emissivity profile, respectively. The increased displacement between the FCs in R and z co-ordinates compared to the current set-up-which was devised without the consideration of this diagnostic technique-enables enhanced sensitivity to changes in the emissivity distribution in the respective directions. Figure 11 shows the predicted variations in FCA ratios, ρ' , from these set-ups for different (R,z) ring-emissivity positions. Here, only geometric effects on the FC detection efficiencies have been considered. These predictions indicate sensitivity to the R of the emissivity distribution for the FC(R) pair enhanced by roughly an order of magnitude compared with the current set-up, with only a small sensitivity to changing z [and vice-versa for the FC(z) pair]. FCA measurements from such a set-up may therefore be more unambiguously ascribed to specific forward-modelled changes to the emissivity profile. It may also be possible to invert these data to infer emissivity profiles from a multiple-FC set-up. Such a diagnostic would allow for the fast-ion populations resulting from different heating regimes to be studied, as will be necessary at MAST-U with the installation of two further NBI lines [17] and an electron Bernstein wave heating system [18]. It would also be possible to measure kicks and oscillations in plasma z via the associated changes in emissivity profile position.

Shine-through from each NBI beam may be measured simultaneously by positioning FCs in close proximity behind each of the beam-dumps outside the vessel, while maintaining one toroidally-displaced diagnostic for comparison. The high shine-through fusion rates measured from the corresponding beam-dump due to this geometric optimisation would allow contributions from all other beams, as well as all beam-dump fusion contributions to the comparison diagnostic, to be neglected.

In addition to the applications presently discussed, an array of toroidally-displaced FCs may be used to identify localised prompt fast-ion losses via the fusion induced with background deuterium within plasma-facing components. Using an array comprising of at least three FCs, information on the locations

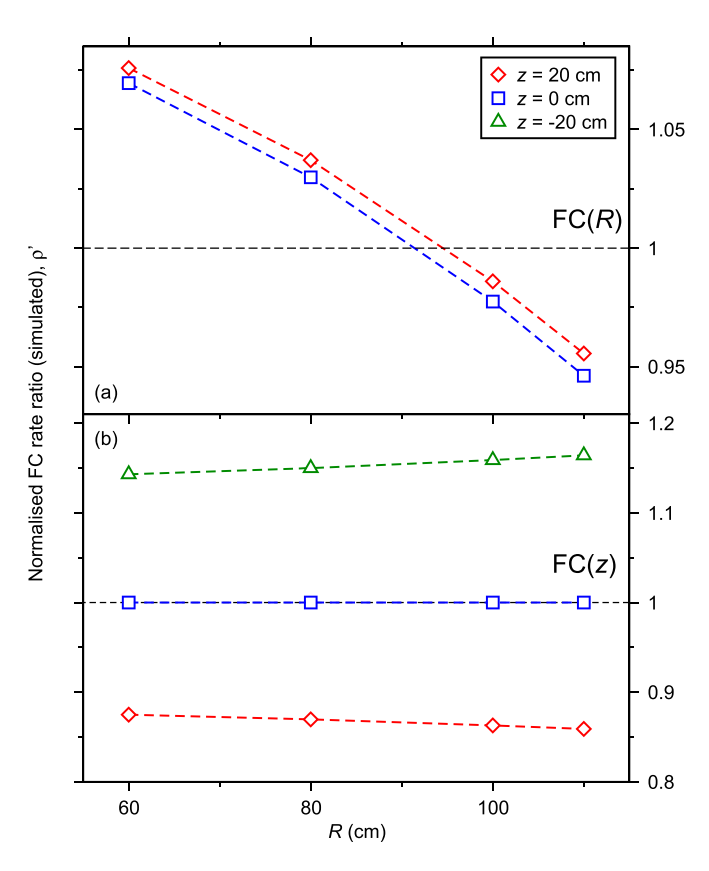


Figure 11. Predicted FCA intensity ratios, ρ' , for two sets of proposed FC positions optimised for measurement of poloidal neutron emissivity profile R [FC(R) (a)] and R [FC(R) (b)]; FC positions shown in figure 3. Calculated with FC detection efficiencies affected only by geometry [N.B. results for R = R = R = R = R cm are same for FC(R)]. Details of the results are as in figure 4.

of such losses may be determined. Such a FCA set-up may also be used to study locking magnetohydrodynamic modes via the toroidal asymmetries they produce in the fast-ion population. For these studies however, as well as others discussed (such as shine-through measurements in the presence of high plasmafusion neutron rates), it may be necessary to have FCA set-ups with reduced noise-signal contributions and higher measurement precision.

To summarise, results from a FCA diagnostic at MAST-U—whereby the data from multiple individual fission chambers are analysed concurrently to study changes in the spatial distribution of fusion—have been presented. Expected shifts in ratios between neutron rates measured by the two FCs have been forward modelled with ring emissivities at different poloidal (*R*,*z*) using MCNP simulations. The measured change in FCA ratio between on- and off-axis and off-axis only heated plasmas is consistent with these simulated expectations; considering the shift in poloidal neutron emissivity distribution measured in the NCU. Also, the use of the FCA to measure and quantify the shine-through during discharges has been demonstrated.

The FCA diagnostic would be an attractive prospect for future tokamaks and reactors due to its radiation resistance in situations where high neutron and γ -ray fluxes from D–T fusion reactions render many diagnostics unsuitable. The FCA is also relatively cheap and simple to install and operate, being

located outside the vessel and requiring no lines-of-sight to the plasma.

Data availability statement

The data cannot be made publicly available upon publication because they are not available in a format that is sufficiently accessible or reusable by other researchers. The data that support the findings of this study are available upon reasonable request from the authors.

Acknowledgments

This work has been part-funded by the EPSRC Energy Programme (Grant No. EP/W006839/1). To obtain further information on the data and models underlying this paper please contact PublicationsManager@ukaea.uk. This work has also been funded by the US DoE (Grant Nos. DE-SC0019007 and DE-SC0001157).

Appendix. Quantified shine-through measurement

Assume that the total neutron rates measured in the FCs, I, derive from two sources: the toroidally-symmetric emissivity from the confined plasma, I_p , and that from the fusion reactions induced by shine-through at the beam-dump, I_b ,

$$I = I_{\rm p} + I_{\rm b}.\tag{A.1}$$

The ratio of neutron rates measured in FCs 1 and 2 is then given as,

$$r = \frac{I_{p2} + I_{b2}}{I_{p1} + I_{b1}}. (A.2)$$

The ratios for purely plasma or beam - dump fusion are assumed constant,

$$r_{\rm p} = \frac{I_{\rm p2}}{I_{\rm p1}}, \quad r_{\rm b} = \frac{I_{\rm b2}}{I_{\rm b1}}.$$
 (A.3)

These values may be measured experimentally using: high-density discharges, ensuring negligible contributions from shine through, for r_p ; and beam-into-gas/vacuum shots with $B_t = 0$ for r_b . Substitute A.1 and A.3 into A.2, normalise ratios to r_p (to give r' and r'_b), and rearrange to give,

$$I_{b2} = I_2 \frac{(1 - 1/r')}{(1 - 1/r'_b)}.$$
 (A.4)

The proportion (%) of full-energy beam shine-through may be given in terms of the measured neutron rate produced by beam-dump fusion, compared with the maximum value resulting from 100% shine-through alone,

Shine – through (%) =
$$100 \frac{I_{b2}}{I_{0.b2}}$$
. (A.5)

This is then substituted into A.4 to give the shine-through as a function of ratio, r', and total neutron rate, I_2 , measured throughout the plasma discharge,

Shine – through (%) =
$$\frac{100I_2}{I_{0,b2}} \frac{(1-1/r')}{(1-1/r'_b)}$$
. (A.6)

ORCID iDs

E Parr © 0000-0001-6204-4461 K G McClements © 0000-0002-5162-509X C A Michael © 0000-0003-1804-870X M Cecconello © 0000-0002-2571-1920 T Wilson © 0009-0001-4343-834X

References

- [1] Nishitani T, Kasai S, Johnson L C, Ebisawa K, Walker C and Ando T 1999 Rev. Sci. Instrum. 70 1141
- [2] Yamauchi M, Nishitani T, Ochiai K, Morimoto Y, Hori J, Ebisawa K, Kasai S and Walker C 2003 Rev. Sci. Instrum. 74 1730
- [3] Ishikawa M, Kondoh T, Nishitani T and Kusama Y 2008 Rev. Sci. Instrum. 79 10E507
- [4] Harrison J R et al 2019 Nucl. Fusion 59 112011
- [5] Vincent C, Allan S Y, Naylor G, Stephen R, Bray S, Thornton A and Kirk A 2022 Rev. Sci. Instrum. 93 093509
- [6] Allan S Y 2024 Personal communication
- [7] Werner C J et al 2017 MCNP users manual-code version 6.2 Los Alamos National Laboratory 746
- [8] Forrest R, Capote R, Otsuka N, Kawano T, Koning A J, Kunieda S, Sublet J-C and Watanabe Y 2012 INDC(NDS)-0628 IAEA Vienna
- [9] Morris W et al 2014 IEEE Trans. Plasma Sci. 42 402
- [10] Cecconello M et al 2023 Plasma Phys. Control. Fusion 65 035013
- [11] Goldston R J, McCune D C, Towner H H, Davis S L, Hawryluk R J and Schmidt G L 1981 J. Comput. Phys. 43 61
- [12] Pankin A, McCune D, Andre R, Bateman G and Kritz A 2004 Commun. Comput. Phys. 159 157
- [13] Cecconello M, Sperduti A, Fitzgerald I, Conroy S, Holm S J and Weiszflog M 2018 Rev. Sci. Instrum. 89 101110
- [14] Ziegler J F, Ziegler M D and Biersack J P 2010 Nucl. Instrum. Meth. B 268 1818
- [15] Bosch H-S and Hale G M 1992 Nucl. Fusion 32 611
- [16] Scannell R, Walsh M J, Dunstan M R, Figueiredo J, Naylor G, O'Gorman T, Shibaev S, Gibson K J and Wilson H 2010 Rev. Sci. Instrum. 81 10D520
- [17] Barrett T R, Jones C, Blatchford P, Smith B, McAdams R and Wood N 2011 Fusion Eng. Des. 86 789
- [18] Webster H et al 2023 EPJ Web Conf. 277 04004